Quantitative proteomics of caveolin-1-regulated proteins: characterization of polymerase I and transcript release factor/CAVIN-1 IN endothelial cells

Article *in* Molecular & Cellular Proteomics · October 2010

DOI: 10.1074/mcp.M110.001289 · Source: PubMed

CITATIONS
36

READS
246

10 authors, including:

Alberto Dávalos
Madrid Institute for Advanced Studies
124 PUBLICATIONS **5,727** CITATIONS
SEE PROFILE

Carlos Fernández-Hernando
Yale University
235 PUBLICATIONS **10,040** CITATIONS
SEE PROFILE

Grzegorz Sowa
University of Missouri
27 PUBLICATIONS **1,473** CITATIONS
SEE PROFILE

Michelle Lin
CRISPR Therapeutics
32 PUBLICATIONS **2,548** CITATIONS
SEE PROFILE

MCP Papers in Press. Published on June 28, 2010 as Manuscript M110.001289

Quantitative proteomics of caveolin-1 regulated proteins: Characterization of PTRF/Cavin-1 in endothelial cells

Alberto Dávalos[1], Carlos Fernández-Hernando[2], Grzegorz Sowa[3], Behrad Derakhshan [1], Michelle I. Lin[1], Ji Y. Lee[4] , Hongyu Zhao[4], Ruiyan Luo[4], Christopher Colangelo[5], William C. Sessa[1*]

[1] Department of Pharmacology and Vascular Biology and Therapeutics Program, Yale University School of Medicine, New Haven, CT, USA.

[2]Departments of Medicine and Cell Biology, and the Leon H. Charney Division of Cardiology, New York University School of Medicine, New York, NY, USA.

[3] Department of Medical Pharmacology and Physiology, University of Missouri, Columbia, Missouri 65212, USA.

[4] WM Keck Foundation Biotechnology Resource Laboratory, Biostatistics Resources, Yale University, New Haven, CT, USA.

[5]WM Keck Foundation Biotechnology Resource Laboratory, Mass Spectrometry Resources, Yale University, New Haven, CT, USA.

Correspondence should be addressed to: William C. Sessa, phone: +12037372291; fax: +1 203 737 2290; william.sessa@yale.edu

Running title: Cavin-1 regulates endothelial cell functions

Keywords: iTRAQ, quantitative proteomics, membrane raft, caveolae, PTRF/cavin-1, endothelial cells, nitric oxide

Abbreviations:

EC, endothelial cells

Cav-1, caveolin-1

Cav-2, caveolin-2

PTRF/Cavin-1, polymerase I and transcript release factor

DRM, detergent resistance membranes

SDPR/Cavin-2, serum deprivation protein response

NS, negative non-silencing control

HUVEC, human umbilical vein endothelial cells

BAEC, bovine aortic endothelial cells

ABSTRACT

Caveolae are organelles abundant in the plasma membrane of many specialized cells including endothelial cells (EC), epithelial cells and adipocytes and in these cells, caveolin-1 (Cav-1) is the major coat protein essential for the formation of caveolae. To identify proteins that require Cav-1 for stable incorporation into membrane raft domains, a quantitative proteomic analysis using iTRAQ was performed on rafts isolated from wild-type and Cav-1 deficient mice. In three independent experiments, 117 proteins were consistently identified in membrane rafts with the largest differences in the levels of Cav-2 and in the caveolae regulatory proteins, Cavin-1 and Cavin-2. Since the lung is highly enriched in EC, we validated and characterized the role of the newly described protein, Cavin-1, in several cardiovascular tissues and in EC. Cavin-1 is highly expressed in EC lining blood vessels and in cultured EC. Knockdown of Cavin-1 reduces the levels of Cav-1 and -2 and weakly influenced the formation of high Mw oligomers containing Cav-1 and -2. Cavin-1 silencing enhances basal nitric oxide release from EC, but blocks pro-angiogenic phenotypes such as EC proliferation, migration and morphogenesis in vitro. Thus, these data support an important role of Cavin-1 as a regulator of caveolae function in EC.

INTRODUCTION

Caveolae have been extensively studied and shown to play an important role in the regulation of many cellular functions including cell signaling, vesicular transport and lipid metabolism. Caveolae are especially abundant in adipocytes, endothelial cells (EC), fibroblasts and smooth-muscle cells (1-3) and there is evidence that the loss of caveolae function may contribute to dyslipidemia, muscular dystrophy, cancer, diabetes and cardiovascular diseases (1, 4-7). Caveolae are a subset of lipid rafts characterized by a particularly high content of cholesterol and sphingolipids that contain the protein, caveolin. There are three isoforms of caveolin, caveolin-1 (Cav-1), -2 (Cav-2) and -3 (Cav-3) that have been extensively studied (1, 4). Cav-1 and Cav-3 are required for caveola formation in different tissues (8-10). While Cav-2 is not required for caveolae formation, per se, (11) it regulates aspects of lung morphogenesis. Although the roles of caveolins in caveolae formation are well known, the requirement of other proteins regulating caveolin function and thus caveola formation has been recently addressed (12-14).

In order to identify proteins that stably interact and are regulated by Cav-1, we used an unbiased, proteomics approach using isobaric tagging for relative and absolute quantification (iTRAQ). iTRAQ is a powerful quantitative proteomic tool for the relative quantification of proteins in complex mixtures by mass spectrometry (15) and this technology has been successfully employed for global comparison of protein expression in many cells systems and in different tissues (16-17). As caveolae and Cav-1are present in the endothelium lining all blood vessels of the body (18-19), and play an important role in the regulation of several endothelial cell (EC) functions (8, 20-22), we examined the protein expression profile of proteins localized in detergent resistant membranes (DRM) prepared from the lungs of wild-type (WT) and Cav-1

KO mice via iTRAQ labeling and multidimentional LC and MS/MS analysis. Here, we show that Cav-1 is required for the appearance of Cav-2, polymerase I and transcript release factor (PTRF) /Cavin-1 and serum deprivation related protein (SDPR; aka Cavin-2) in isolated DRM from lungs confirming the initial discovery of these proteins as regulators of Cav-1 dependent caveolae function. Isolated as a functional complex in cells, Cavin-1 co-fractionates into DRM with Cav-1 and -2 but Cavin-1 forms high molecular weight homo-oligomers separated from Cav-1 and Cav-2 using sedimentation velocity gradients. Knockdown of Cavin-1 in EC affects several functions including nitric oxide production, migration and morphogenesis. Thus, Cavin-1 has a critical role in regulating several aspects of caveolae function in EC.

EXPERIMENTAL PROCEDURES

Isolation of detergent insoluble rafts from lung tissue

Membrane rafts were isolated as previously described (23) with minor modifications. Briefly, lungs from three mice (female, 8-10 week old) were isolated and tissue was mince with scissors on ice and transferred onto a tube. Lungs were adjusted up to 3 mL volume with cold Mes-buffered saline (MBS; 25 mM Mes, pH 6.5, and 150 mM NaCl) containing protease inhibitors and homogenized using a Dounce homogenizer. Homogenate was adjusted to 3.25 mL with MBS and 3.25 mL of MBS containing 2% Triton X-100 was added and homogenized. Sample was rocked for 30 min at 4^{o}C . Next, the suspension was mixed with an equal volume of 85% sucrose in MBS. 2 mL of the 42.5% sucrose suspension was overlaid with 8 mL of 35% sucrose and 2 mL of 5 % sucrose in an ultracentrifuge tube, and centrifuge for 18 h at 35000 rpm at 4 ^{o}C in a SW40 rotor. Twelve fractions of 1 mL was collected from the top, mixed with SDS/PAGE loading buffer, and equal volumes were loaded and run on the SDS/12% PAGE, and Western blotted. For iTRAQ analysis, fractions 1 and 2 were pooled together and sucrose was diluted to ½ with cold water and split in SW28 rotor untracentrifuge tubes and centrifuge for 90 min at 28,000 rpm at 4 ^{o}C. Pellet were pooled and precipitated with chloroform:methanol and submitted to iTRAQ analysis

Protein Digest, iTRAQ^{TM} Labeling, and LC-MS analysis

Two hundred micrograms of protein pellets were dissolved in the solution buffer, reduced, and cysteines were blocked as described in the protocol of the iTRAQ kit (Applied Biosystems). In total three biological replicates were performed and each 4-plex iTRAQ had an experimental (technical) replicate for both the wild-type and knockout samples. Briefly, after overnight trypsin

digestion, 100 µg of samples were labeled with iTRAQ tags as follow: two WT samples with iTRAQ 114 and iTRAQ 115 reagents respectively, and two Cav-1 KO samples with iTRAQ 116 and iTRAQ 117 reagents, respectively. Labeled samples were pooled and purified using a strong cation exchange (SCX) column (Applied Biosystems) and separated into 20 fractions. *QSTAR XL LC-MS/MS Analysis*. Each cation-exchange fraction was dried and resuspended in 10 µl 0.1% formic acid in preparation for RP-LC with the LC Packing's Ultimate workstation allowing us to pre-concentrate the 10 µl samples on a Waters 5 mm C18 Symmetry 300 trap column. The individual peptides were then separated at a flow rate of 450 nl/min on an in-line 100 µm x 15 cm Waters Atlantis C18 column equilibrated with 0.5% acetic acid, 5% acetonitrile and eluted with a 60 min acetonitrile gradient. Data collection was performed by electrospray Ionization of the eluent with data-dependent acquisition on a Applied Biosystems API Q-Star XL mass spectrometer

Data analysis and statistics

Each of the QSTAR XL mass spectrometer spectra files (*.wiff) was processed with MASCOT Distiller version 2.1 and the resulting peak lists were combined and database searched using MASCOT Server 2.1. The search parameters included trypsin with one miss cleavage, static modifications carbamidomethyl (cys) and iTRAQ reagents (N-term, K), and variable modifications for oxidation (met). Data analysis on the resulting LC/MS and MS/MS datasets is accomplished using a dual processor Dell 650 Workstation. The search results for each fraction were analyzed using the IPI mouse 3.27 (released March 27, 2007 and contained 53,831 seqeunces). After MASCOT analysis, Peptide and ProteinProphet (Institute for Systems Biology) analysis (24-25) was performed using the Trans-Proteomic Pipeline version 2.7 MIST rev.2, Build 200601091318. Peptide and Protein Prophet computes the probabilities for both

individually searched peptides and the resulting proteins. The protein validation was performed using both PeptideProphet and ProteinProphet values such that a protein is validated if it has at least two top ranked peptides with each peptide probability score being above 95% and above 94% (Supplemental Figure S1) ProteinProphet probability cutoff corresponding to a 0.004, 0.003, 0.003 false positive error rate for all three biological replicates (Supplemental Table S1). Finally, all TPP identifications are submitted to Yale Proteomics Expression Database (YPED) web site for further user analysis.

iTRAQ Quantiation and secondary protein identification was performed using the Paragon^{TM} search algorithm (26) in ProteinPilot 2.0 software. IPI mouse 3.27 (released March 27, 2007) database was used using ‘‘thorough search’’. The ‘‘iTRAQ 4plex peptide labeled’’ sample type and a ‘‘biological modification ID focus’’ were selected in the analysis method. Trypsin was selected as the digestion enzyme with cysteine alkylation by methyl methane thiosulfonate as a modification. Raw data that included, but was not limited to, reporter ion peak areas, reporter ion peak area error, peptide assignment, and confidence was exported from ProteinPilot (tab-delimited) without ProteinPilot’s auto bias correction applied (non-normalized data) so we could perform quantile normalization as described below. The tab delimited ProteinPilot results were then uploaded into our Yale Protein Expression Database (YPED). For secondary protein identification, each protein had to have also been identified by Paragon and had two or more identified peptides and a ProteinPilot Confidence Score >2 (99% confidence level). To ensure that we only compared data that ProteinPilot includes in its quantitation analysis, peptides had to be classified as ‘‘used’’, which requires the presence of an iTRAQ label and at least one valid iTRAQ reporter ion ratio. Additionally, ProteinPilot only uses high-quality reporter ions for the peak area measurements to calculate iTRAQ peptide ratios. To remove low-

intensity reporter ion ratios from the exported raw data sets, we used ProteinPilot's non-modifiable criterion, which requires that valid iTRAQ reporter ion ratios must contain two iTRAQ reporter ions with a summed S/N ratio >9 to be included in the analysis. All raw data (mzXML), peak list (mgf), MASCOT search results (dat), ProteinPilot Search results, PeptideProphet (pepXML), and ProteinProphet (protXML) files are publicly available through http://yped.med.yale.edu/repository (ACCESS CODE - **aSKezE**).

YPED has additional features, which enabled us to perform sample comparisons and Panther Classification. Quantile Normalization of the iTRAQ data was performed to correct the variation of the protein abundance using statistical package R. Principal Components Analysis was used to examine the consistency of the technical replicates and biological replicates. Among 425 unique proteins observed in the experiments, there were 117 proteins identified in common through the experiments. A cutoff was set at 0.8 for down-regulated proteins and 1.2 for up-regulated proteins as reported for other works (27-28). Protein expression values from technical and biological replicates are analyzed under the ANOVA model. Nitric oxide production was compared using t-test and pairwise comparisons by the Mann-Whitney test. Effects on protein or gene expression were analyzed by ANOVA and comparisons between each experimental condition and the control were made by the confidence interval method. All values are presented as the mean ± SEM, and a *P* value of less than 0.05 was considered statistically significant. Calculations were performed using the Graph Prism 4 software (San Diego, CA) or SigmaStat Statistical Analysis, System V. 1.00 (Jandel Corporation, San Rafael, CA).

Antibodies

Mouse SDPR antibody was a kind gift from Prof. R.G.W. Anderson (U. of Texas Southwestern Medical Center). The following antibodies were obtained from commercial sources: rabbit anti-

caveolin (610060; BD), mouse anti-caveolin 2 (610685; BD), mouse anti-HSP90 (610419, BD), mouse anti-eNOS (610297; BD), mouse anti-PTRF (611259; BD), rabbit anti-PTRF (A301-271A, Bethyl Laboratories), rabbit anti-PTRF (A301-270A; Bethyl Laboratories), rabbit anti-phospho-eNOS (36-9100; Zymed), rabbit anti-NOS (sc-653; Santa Cruz Biotechnology), rabbit anti-caveolin 1 (sc-894 ; Santa Cruz Biotechnology); mouse anti-caveolin 1 (NB 100-615; Novus Biologicals); mouse anti-SDPR (H08436-B01; Novus Biologicals)

Cell culture

COS-7, HEK 923, and EAhy.926 were maintained in high-glucose DMEM supplemented with 10% FBS, L-glutamine, antibiotics, and HAT supplement (EAhy.926) at 37°C in a humidified atmosphere of 5% CO_2. HUVECs were maintained in M199 media and only passage 2-3 were used for experiments. Mouse lung endothelial cells (MLEC) were isolated from WT, Cav-1 KO, Cav-1 RC and Cav-1 TG mice were maintained in EBM-2 media supplemented with EGM-2 MV SingleQuots.

Immunufluorescence microscopy

After dissection, aorta (from 8-wk-old mice) were fixed with 4% paraformaldehyde for 10 min at 4°C, and then dehydrated in 15% sucrose overnight at 4°C. The vessels were then embedded in OCT (Sakura) and frozen. Serial 10-µm sections were blocked with 3% goat serum. Slides were incubated with either rabbit anti-Cavin-1 (Bethyl) or rabbit anti-Cav-1 antibody (BD) 1:100 dilution each at 4°C overnight. Alexa Fluor 488 or 594 anti–rabbit IgG (Invitrogen) was used as secondary antibody (1:250 dilution; at room temperature for 1 h). For cells, COS-7 and EA.hy.926 cells grown on coverslips were fixed with 4% PFA for 5 min, rinsed with PBS, permeabilized with 0.1% Triton X-100 for 10 min, washed with PBS, and blocked with 5% goat

serum for 45 min at room temperature. Cells were incubated with the primary antibodies (diluted 1:200) overnight at 4°C and washed twice with blocking solution, followed by a 45-min incubation with appropriate secondary antibodies conjugated to immunofluorescent dyes Alexa Fluor 488 or Alexa Fluor 594 (diluted 1:250) at room temperature. After washing three times, coverslips were mounted on slides with Gelvatol/DAPI (Sigma-Aldrich) and analyzed with an epifluorescence microscope (Axiovert; Carl Zeiss MicroImaging, Inc.). Images were acquired using a charge-coupled device camera (Axio; Carl Zeiss MicroImaging, Inc.). Analysis of different images was performed using Openlab software (Improvision) after subtracting background.

Real time RT-PCR analysis

Total RNA was extracted with Trizol reagent using the RNeasy columns (Qiagen). Reverse transcription was performed using 2 µg of total RNA using TaqMan reverse transcription reagents (Applied Biosystem) , and quantitative PCR was performed using iQ SYBR Green Supermix (Bio-rad) according to the manufacturer's protocol on an iCycler quantitative PCR analyzer (Bio-Rad).

siRNA, plasmids and cell transfection

Cavin-1 target sequence against 5'-CAACTTTAAAGTCATGATCTA-3' was obtained from QIAGEN (HP guaranteed siRNA) and a scrambled siRNA was used as a negative nonsilencing control (NS) (5'-AATTCTCCGAACGTGTCACGT-3'). 50% of confluency ECs were transfected with RNAi construct (75 nM) using Oligofectamine (Invitrogen) according to the manufacturer's instructions for 8h in Opti-MEM (Invitrogen) and then incubated in full medium for 48 h. A second 8h of transfection was performed and then either HUVEC or EAhy.926 growth medium,

was added for additional 48h. After reaching 40% confluency in a 6-well tissue culture plates, HEK 293 or COS-7 cells were transfected with 1 μg of cDNA plasmid for 8h with FuGENE 6 reagent in Opti-MEM. Then, media was replaced with DMEM 10% FBS for 36 h. cDNAs for human Cav-1 HA-tagged or Cav-2 myc-tagged were constructed and subcloned in pcDNA3 vector (Invitrogen) .

Non-detergent based fractionation and sucrose gradient

Cells (150-mm dish) were washed twice with PBS and scraped into 2 ml of ice-cold 500 mM sodium carbonate, pH 11, supplemented with 1 mg/ml protease inhibitor cocktail (Roche), Dounce homogenized, and sonicated (three 20-s bursts at 30% of maximal power). The homogenate was then adjusted to 42.5% sucrose by the addition of 2 ml 85% sucrose prepared in MBS (25 mM MES, pH 6.5, and 0.5 M NaCl) and placed at the bottom of an ultracentrifuge tube. A 5–30% discontinuous sucrose gradient was formed (3 ml of 5% sucrose and 5 ml of 30% sucrose, both in MES containing 250 mM sodium carbonate) and centrifuged at 35,000 rpm for 18 h in a SW40 rotor (Beckman Coulter). Twelve gradient fractions (1 ml) were collected from the top, mixed with SDS/PAGE loading buffer, and equal volumes were loaded and run on the SDS/12% PAGE, and Western blotted. The percentage of total proteins in different fractions was determined by densitometry and plotted as percentage of total protein (NIH program).

Immunoprecipitation and Western blot analysis

Cells lysed were solubilized with either 60 mM octylglucoside or 1% Triton X-100 for 1 h at 4 °C and immunoprecipitation was performed on 500 μg of total cell protein using (4μg) antibodies or nonspecific normal rabbit IgG for 2 h at 4°C. Protein G Sepharose (Sigma) was then added and incubated for 1 h. Beads were precipitated by centrifugation and the supernatant

was collected. The immune complexes were washed three times with immunoprecipitation buffer and both supernatant and immunoprecipitates were boiled in SDS sample buffer before resolving by SDS-PAGE and Western blotted using the antibodies described above

Velocity gradient centrifugation and cross-linking

Velocity gradient centrifugation. Influence of cavin in caveolins oligomerization was performed as described for caveolin 1(29) and caveolin 2 (30) with minor modifications. Briefly, sample were dissociated with 700 µl of Mes-buffered saline (MBS; 25 mM Mes, pH 6.5, and 150 mM NaCl) plus 60 mM *n*-octyl-β-D-glucopyranoside). Solubilized material was then loaded atop a 5-50% linear sucrose gradient (12 ml) and centrifuged at 42,000 rpm for 16 h in a SW-40 rotor (Beckman Instruments, Palo Alto, CA). After centrifugation, twelve 1mL gradient fractions were collected from the top mixed with SDS/PAGE loading buffer, and equal volumes were loaded and run on the SDS/12% PAGE, and Western blotted. Molecular mass standards for velocity gradient centrifugation were as follows: carbonic anhydrase (29 kDa), BSA (66 kDa), β-amylase (200 kDa), apoferritin (443 kDa), and thyroglobulin (669 kDa) (Sigma). Linear sucrose gradient was performed with a 5% and 50% sucrose solutions prepared with MBS/60 mM octyl gucoside using a Gradien Station *ip* (BioComp Instruments). *Chemical cross-linking*. Chemical cross-linking was performed in vivo on intact cells as previously described (31). Confluent cells were washed with KCl/HEPES buffer (90 mM KCl, 50 mM HEPES, pH 7.5) and incubated with DSP at a final concentration of 2 mM. After incubation for 30 min at room temperature, the reaction was termined by adding Tris-HCl 20mM (pH 8), glycine 50mM. Cells were lysed followed by separation on a 4-20% continuous gradient precast gels (Invitrogen) and western blot analysis.

NO release analysis

After 96h of Cavin-1 silencing, the media was removed and the cells were supplemented with serum-free DMEM media for 8 h. Nitrite (NO_2^-) was measured by a NO-specific chemiluminescence analyzer (Sievers) as previously described (32). NO release was normalized to protein levels and values are expressed as μmol nitrite/mg cell protein.

Proliferation assay

HUVEC were seeded in 12-well plates and treated with siRNA sequences as descrived above. At the indicated times cells were trypsinized and counted using a hemocytometer. Viability was determined by Trypan blue dye exclusion.

Cell migration assay

Cell migration was evaluated with a modified Boyden chamber (Corning). Transwell inserts were coated with a 0.1% gelatin solution at 4°C overnight. After cavin silencing, subconfluent ECs were serum starved overnight and suspended in DMEM media containing 0.1% FBS and 100 μL of cell suspension containing 50 $x10^3$ ECs were added to the upper chamber. The bottom chamber contained either 50 ng/mL VEGF, 200 nmol/L S1P or 10% FBS prepared in DMEM media. After 5 hr incubation at 37°C, cells on both sides of the membrane were fixed and stained with the Diff-Quik staining kit (Baxter Health). Non-migrated cells were removed with a cotton swab and the average number of migrated cells per field from 5 high-power (×400) fields was counted.

Tube formation assay

After Cavin-1 silencing, 60 $x10^3$ ECs were seeded on top in a 24-well plate coated with growth factor reduced Matrigel (BD Biosciences) in DMEM containing 0.1% FBS with or without 50 ng/mL VEGF or 200 nmol/L S1P. After 5 h incubation at 37°C, sprout length of capillary-like

structures was quantified by measuring the mean cumulative tube length using OpenLab Software (Improvision) in a computer assisted microscope (Axiovert; Carl ZeissMicrolmaging, Inc.). Images were taken in five fields for each well and each condition was performed in triplicate per experiment.

RESULTS

Quantitative proteomics examining proteins in lipid rafts isolated from wild-type (WT) and Cav-1 KO lungs

In order to examine the proteins that interact with and stabilize caveolin-1, detergent resistant membranes (DRM or raft domains) were isolated using sucrose gradient fractionation from lung tissues prepared from WT and Cav-1 KO mice. Sucrose gradient centrifugation of raft domains (fractions 1 and 2 from top of gradient reflecting glycolipid and cholesterol rich fractions) verified the distribution of Cav-1 and flotillin-1 in WT extracts and flotillin-1 in KO extracts (Flot-1; Fig. 1A, left panel). The raft fractions were pooled, protein precipitated with methanol/chloroform, reduced, alkylated, trypsinized and labeled with iTRAQ reagents for analysis by LC/MS/MS. As variations in protein isolation, enzymatic digestion and isotopic labeling can contribute to the variation in iTRAQ data, consistency of the protein abundance within an experiment or across experiments can be a concern. Three independent experiments using four different isotopic labeling reagents for each experiment were performed (Supplemental Fig. S2A). Although the ratio of WT to KO obtained across experiments was highly correlated (r^2=0.909), some variation within an experiment and across experiments was observed (Fig. S2B) and quantile normalization was performed to minimize variation. As depicted in Supplemental Fig. S2C, the alignment of the protein abundance for KOs labeled with 116 reagent and 117 reagent within an experiment was improved after normalization. Principal Components Analysis (PCA) was performed to examine the clustering patterns of the technical replicates and biological replicates (Fig. S2D). 70.99% of the data were explained by the first component and 15.51% by the second component. Actin gamma cytoplasmic 1 with score = -9.29 and probable phospholipid-transporting ATPase IA with score = 5.04 are the top two

proteins driving the separation along the first principal component. Although the variation due to protein isolation and enzymatic digestion still exists, the variation in isotopic labeling was corrected.

After protein identification and relative quantification using the criteria (described in the "Experimental Procedures"), around 200 proteins were identified from each of the three sets of independent experiments performed (238, 178, 223 proteins from experiments 1-3, respectively). Protein lists generated from the three experiments were combined and analyzed and 117 proteins were in common in all experiments (Fig. 1B). With the 117 proteins common to the three DRM iTRAQ replicates the $\log_2$ transformed values of the normalized data from ratio WT/KO and internal replicate were performed and illustrated for the means of the relative protein expression levels (Figure 1C). Statistical analysis of the relative expression of these proteins was performed and the fold-change was calculated. Ratio of average expression in KO and in WT was defined as fold changes. The average expression in KO and in WT was calculated as average of mean expression of the technical replicates across the biological replicates. These resulted in a list of 61 proteins that showed marked changes in lipid rafts isolated from WT versus Cav-1 KO mice ($p<0.05$) as listed in Tables 1 and 2. Additionally, 56 proteins showed no significant changes (Supplemental Table S2) in WT versus Cav-1KO, suggesting that enrichment of these proteins is not dependent on the absence or presence of Cav-1. However, we do not discard that some of these proteins may be contaminants that partially copurify with DRM/raft preparations(33-34), as electron transport proteins, hemoglobins and histones proteins. To confirm the iTRAQ results, we performed semi-quantitative Western blotting on certain proteins observed to be reduced in caveolae/lipid raft fractions from Cav-1 KO mice and rationalized based on the literature. As seen in Fig 1D, the levels of Cavin-1, serum deprivation-response protein (SDPR aka Cavin-2)

and Cav-2 (a known interacting protein stabilized by Cav-1), are reduced in raft fractions from Cav-1 KO mice in accordance with our proteomic data set (Table1). The loss of Cavins-1 and -2 are consistent with data suggesting these proteins regulate aspects of caveolae formation (12-14, 35-36). As seen Fig 1E, Cavin-1, Cavin-2 and Cav-2 levels are reduced in total cell lysates prepared from lung tissue supporting the idea that the reduction of Cavins and Cav-2 in raft fractions is due to destabilization of the protein complex.

Cavin-1 is enriched in blood vessels and endothelial cells and is regulated by Cav-1

Cav-1 in blood vessels is critical for mechanosensing (22) and vascular function (20, 37), thus, we examined the localization of Cavin-1 in intact mouse aorta and cultured endothelial cells (EC). As seen in Fig 2A, using immunofluorescence microscopy, Cavin-1 is highly expressed in all layers of the blood vessel (top panel) and the loss of Cav-1 reduces immunoreactive Cavin-1 throughout the vessel (bottom panel). To examine the relationship between Cav-1 and Cavin-1 levels in more detail, we examined the protein levels in heart, lung and aortic extracts from WT, Cav-1 KO and Cav-1 RC mice. Cav-1 RC is a strain of mice where global Cav-1 KO mice were reconstituted with an endothelium specific transgene of Cav-1 (20, 22, 38). As seen in Fig 2B, the loss of Cav-1 markedly diminished Cav-2 levels and partially reduced Cavin-1 levels in all tissues examined. Re-expression of Cav-1 in EC (Cav-1 RC) dramatically rescued Cav-2 in the lung and aorta and to a lesser extent the heart while modestly increasing Cavin-1 levels in lung and aorta, but not the heart. Since lungs have the highest abundance of EC in the body, the re-expression of Cav-1 in EC stabilizes Cav-2 and Cavin-1 best in this tissue, followed by the aorta. The lack of significant rescue in the heart is likely due to the expression of Cav-1/Cavin-1 in cardiac fibroblasts and the high abundance of Cav-

3/Cavin-1 in cardiac myocytes, the primary cell type in the heart, where the re-expression of Cav-1 in EC would not be expected to rescue the loss of Cavin-1 in cardiac fibroblasts or myocytes (39).

To examine the effects of Cav-1 on Cav-2 and Cavin -1 levels in a cell that expresses all three proteins, lung (EC) were cultured from the three strains of mice. Similar to data in lung lysates, the loss of Cav-1 markedly reduced Cav-2 levels and partially reduced Cavin-1 levels (by ≈ 60%.; see inset). Again, reconstitution of Cav-1 strongly enhanced the levels of Cav-2 and partially enhanced Cavin-1 levels(Fig 2C). These data suggest that the stability of Cavin-1 in cells may be regulated differently than that of the Cav-1/ Cav-2 complex perhaps due to independent trafficking of caveolins versus Cavin in cells resulting in less than stoichiometric interactions of Cavin-1 with the caveolins.

Next, we determined the distribution of Cavin-1 in isolated EC using sodium carbonate lysis and a discontinuous sucrose gradient to separate buoyant membranes (enriched in Cav-1; fractions 2-4) from bulk cellular proteins (fractions 8-12) . As depicted in Figure 2D (top panel), Cavin-1 is present in raft (fractions 2 and 3) and non-raft fractions (8-12) and co-distributes with Cav-1, Cav-2 and eNOS. The presence of caveolins and Cavin-1 in non-raft membranes (Fig 1D and 2D) likely reflects the distribution of these proteins in domains distinct from rafts membranes. These proteins have also been localized to Cav-1 positive endocytic vesicles (40), newly assembled caveolins en route to the plasma membrane (41) and Cavin-1 may also be found in other subcellular fractions (42). The loss of Cav-1 (Cav-1 KO, middle panel) reduces Cavin-1 and Cav-2 levels, while eNOS remains unchanged. As observed (Fig. 1D and 2D), Cav-2 is drastically reduced in both raft and non-raft fractions while Cavin-1 protein levels are mainly reduced in raft fractions relative to non-raft fractions. Reconstitution of Cav-1 (Cav-1 RC;

bottom panel), increases the recovery of Cavin-1 and Cav-2 in light membranes indicating that Cavin-1 is a membrane raft constituent that co-localizes with Cav-1 and Cav-2 in ECs.

Finally, to examine if Cav-1 overexpression (on a WT background) in EC increases Cavin-1 levels, EC from mice that transgenically overexpress Cav-1 in EC (43) were isolated and assayed for the levels of Cavin-1 and caveolins. Transgenic overexpression of Cav-1 increases basal levels of Cavin-1, but not caveolin-2 levels (Figure 2E).

Role of Cavin-1 on Cav-1 and Cav-2 in EC

Cavin-1 is a critical component of caveola and reducing its levels decreases global caveolin levels and caveolae formation in all tissues examined to date (12-14) however, the role of Cavin-1 in EC have not been examined. To test the functions of Cavin-1 in EC, Cavin-1 levels were suppressed using RNAi. Two different RNAi sequences were initially tested in EAhy.926 cells (a human EC line that have ample Cav-1 and caveolae by EM). A time-course of Cavin-1 silencing showed a reduction in Cavin-1 expression at 24 hrs, followed by a reduction in Cav-1 and Cav-2 protein levels were observed at a later time point (96 hrs; Fig. 3A and B). siRNA sequence 2 (siRNA-2) reduced Cavin-1 by ≈75% in primary cultures of human umbilical EC (HUVEC) (Fig. 3B) and by ≈60% in primary bovine aortic endothelial cells (BAEC; Fig. S3A bottom panel).These data suggest a kinetic lag exists between the loss of Cavin-1 and quantitative changes in Cav-1/Cav-2 levels and that the changes in caveolins due to the loss of Cavin-1 vary in different EC lines. The reduction in Cavin-1 levels were clearly observable by immunofluorescence microscopy in EC (Fig. 3C). As expected, using sucrose fractionation, the loss of Cavin-1 also reduced its levels in buoyant membranes and the levels of Cav-1 and -2 (Fig 3D) but to a lesser extent than observed for other cells types such as NIH 3T3 fibroblasts (12,

14). After knockdown of Cavin-1, the reduction of Cav-1 and Cav-2 levels were mainly observed in the plasma membrane as imaged via immunofluorescence microscopy (Supplemental Fig. S3B). The reduction in Cavin-1 mRNA levels by RNAi also reduced Cav-1 mRNA and in a lesser extent Cav-2 mRNA levels at later time points (Fig. 3E). It should be noted that the levels of Cavin-1 mRNA levels decreased dramatically in the first 24h after siRNA treatment while the reduction in protein levels were much slower, suggesting that Cavin-1 has a long biosynthetic half life. As previously shown for adipocytes (14), Cav-1 colocalizes with Cavin-1 in the plasma membrane of EC (Fig. S3C).

Next we examined if Cavin-1 existed in a protein complex with caveolins via co-immunoprecipitation (IP) experiments. As shown in Fig. S3D, IP of either Cav-1 or Cav-2 from EC lysates solubilized in β-octylglucoside (OG) buffer resulted in weak, co-immunoprecipitation of Cavin-1 compared to IgG control Ab. Longer exposure of the membrane showed the presence of the band of Cav-1 in the Cavin-1 IP. Using a 1% Triton X-100 buffer, the complex of Cavin-1, Cav-1 and Cav-2 appeared to be better stabilized. To decipher whether this interaction is direct or indirect, we used a recombinant GST-Cav-1 as bait for in vitro binding (44). Fig. S3E shows the expression of GST and several distinct modules of GST- Cav-1 (amino acids 1-61, 61-101, 135-178 and full length 1-178). Incubation of EC lysates with these fusion proteins demonstrated that GST Cav-135-178 is sufficient to interact with endogenous Cav-1 and GST Cav-1 1-178 could interact with Cav-1 and Cav-2, but no interactions were observed with Cavin-1 under these conditions (Fig. S3F). Overall these data confirm previous data showing that the interaction of Cavin-1 with caveolins is likely indirect or dependent on caveolae structure (14).

Cavin-1 exists as a unique oligomer but does not sediment with Cav-1 and Cav-2

It is well recognized that Cav-1 exists as high-molecular-mass homo-oligomers of ≈200 to 350 kDa (29) and Cav-1 is necessary for the hetero-oligomerization of Cav-2 within the isolated complex (44-45). To examine if Cavin-1 is part of this oligomeric complex, we performed velocity sedimentation gradients using a 5-50% linear sucrose gradient, and assessed the flotation of Cav-1, Cav-2 and Cavin-1 using lysates from WT, Cav-1 KO and Cav-1 RC ECs. As seen in Fig 4A, oligomeric Cav-1 and Cav-2 complexes are enriched in high Mw fractions between 150-220 kDa. Surprisingly, Cavin-1 is virtually undetectable in these fractions but resides in a high Mw complex of greater than 669 kDa. Since the predicted Mw of Cavin-1 is 60kDa, this suggests > 10 monomers of Cavin-1 exist in the complex but the complex does not co-sediment with Cav-1 and Cav-2. In the absence of Cav-1, the levels of Cav-2 and Cavin-1 are reduced, but the residual Cav-2 is left shifted (see graph on right) while the oligomerization of Cavin-1 is intact; while reconstitution of Cav-1 in the Cav-1 KO background rescues this phenotype.

Next, we examined if Cavin-1 modulates the oligomerization of Cav-1 and Cav-2 in EC. siRNA knockdown of Cavin-1 (bottom panels) weakly reduces high Mw Cav-1 and Cav-2 oligomers (from fraction 6 onwards), as compared to NS (top panels; Fig. 4B), however, the functional relevance of this is not known. To independently test the possible role of Cavin-1 in caveolin oligomerization, reconstitution experiments were performed in HEK293 cells which exhibit very low levels of Cav-1, Cav-2 and Cavin (Fig. S4A). Transfection of Cav-1 alone resulted in homo-oligomer formation (corresponding to molecular weights of at least 220 kDa) whereas transfection of Cav-2 alone formed lower molecular weight complexes (Fig. S4*B left panel Middle*). As previously shown, co-expression of Cav-1 and -2 results in the incorporation of Cav-2 into high molecular weight oligomers (Fig. S4*B left panel Bottom*). Transfection of

Cavin-1 alone results in the formation of high Mw homo-oligomers, similar to finding in cells endogenously expressed Cavin (Fig. S4*B right panel Top)*. However, co-expression of Cav-1, Cav-2 and Cavin-1 together weakly increased the amount of high Mw oligomeric Cav-1 and Cav-2 (Fig. S4*B right panel Bottom)*, compared to that of Cav-1 and Cav-2 alone. It has been shown that Cavin-1 associates to caveolae after caveolins arrive to the plasma membrane as a preassembled complex and it is possible that Cavin may stabilize caveolin oligomers in the context of the caveolae structure(46). These results are consistent with the slight reduction in high molecular Mw oligomeric Cav-1/ Cav-2 complex after Cavin-1 silencing in ECs (Fig. 4B). Moreover, while Cav-2 alone formed lower molecular weight complexes, co-expression with Cavin-1 (Fig. S4*B right panel Middle)* did not result in the incorporation of Cav-2 into high molecular weight oligomers. To confirm the latter findings, HEK923 cells transfected with either Cav-1, Cav-2 or Cavin were analyzed by confocal imaging. As previously shown, transfection with Cav-1or Cav-2 shows that Cav-1 is found both in the plasma membrane and perinuclear region, while Cav-2 is localized exclusively in the perinuclear region (Fig. S4*C left panels*). Co-transfection of Cav-1 and Cav-2 caused a redistribution of Cav-2 from perinuclear region to plasma membrane (Fig. S4*C third panel*), while contransfection of Cavin-1 with Cav-2 did not influence Cav-2 targeting (Suppl. Fig. 4*C right panel*).

Interestingly in all the above experiments using velocity gradients, Cavin-1 was detected in higher order homo-oligomers, in the absence or presence of caveolins. To test whether oligomeric Cavin-1 exists in intact cells, a cell permeable chemical cross-linking approach was employed as previously described (31). DSP is a membrane permeable cross-linker with an arms length of 12Å that stabilizes high molecular weight oligomers, which can be analyzed by SDS-PAGE and detected by Western blotting. As shown in Fig. 4C in the absence of DSP,

Cavin runs as a 60kDa protein on SDS-PAGE, while in the presence of DSP, different higher order species of Cavin-1 are found. The band at approximately 180kDa is consistent with at least 3 monomers of Cavin-1, while the Mw of the uppers bands are not discernable.

Cavin-1 regulates several EC phenotypes

Endothelial nitric oxide synthase (eNOS) is negatively regulated via an interaction with Cav-1(47-48). To evaluate the functional role of Cavin-1 silencing in EC, eNOS levels and NO release were evaluated. Knockdown of Cavin-1 increased eNOS protein levels and its phosphorylation on S1177 (Fig. 5A) in EAhy.926 and HUVEC. The increase in eNOS levels was accompanied by a trend to increase in eNOS mRNA levels as detected by qPCR (Fig. S5A) and a ≈40% increase in NO levels (measured as NO_2^-) in the media (Fig 5B).

In addition to an effect on eNOS, Cav-1 is important for other aspects of angiogenesis including cell proliferation, migration and morphogenesis, functions important for angiogenesis in vivo. Knockdown of Cavin-1 reduced cell growth, migration and growth factor induced tube formation in response to VEGF and sphingosine-1-phosphate (Fig. 5C-E). Collectively these data indicate that Cavin-1 is necessary for regulation of eNOS function and several angiogenic phenotypes in vitro.

DISCUSSION

The central purpose of this study was to identify proteins that are co-isolated with or require an interaction with endogenous Cav-1 for their fractionation into detergent resistant membranes (DRM) or lipid rafts. To this end, we performed a quantitative comparison of proteins isolated in lipid raft domains in the presence or absence of endogenous Cav-1 using iTRAQ analysis. Up to 290 proteins were identified, some of which have been previously identified in rafts or DRM of cultured EC or other tissues (12, 16, 49-50). After establishing stringent criterion for filtering the peptide data, statistical analysis was performed with 117 proteins reproducibly recovered in DRM from three independent experiments. 25 proteins were significantly reduced and 36 proteins were found to be increased in DRM isolated from Cav-1 KO mice compared WT mice suggesting that the loss of Cav-1 reduces the partitioning and/or expression of some proteins, while increasing the enrichment/expression of others into isolated raft domains. However, as biochemical isolation of membrane microdomains typically never yield absolute homogenous preparation (33), we could not discard copurifying contaminants during the DRM isolation, as those from the mitochondria complex (34, 51). From a biological interest perspective, we validated certain proteins that were reduced following the loss of Cav-1 and our results confirmed the identification of Cavin-1 and Cavin-2 and Cav-2 as Cav-1 interacting proteins in vivo.

It is well appreciated that Cav-1 and Cav-3 are necessary for caveolae formation in mammalian cells. However recent data suggests that certain accessory molecules are necessary for stabilizing Cav-1 or Cav-3 functions and to form a caveolae in specific tissues. Four proteins, recently termed Cavins: Cavin-1 (aka PTRF, Cav pp60), Cavin-2 (SDPR or SDR),

Cavin-3 (protein kinase C delta binding protein or SRBC) and Cavin-4 (PTRF/SDPR family protein or MURC) have been shown to interact with each other and require caveolins for membrane association (35, 52). Very recently, in the context of Cavin-1, Cavin-2 and Cav-1, the loss of either Cavin-1 or Cavin-2 reduces the levels of Cav-1, and overexpression of Cavin-2 is sufficient to stabilize the ternary complex and promote caveolae function. Cavin-1 can directly interact with Cavin-2 in vitro and can form immunocomplexes with Cav-1. Our data support this idea since Cavin-1 co-precipitates with both Cav-1 and Cav-2, and the interaction with Cav-1 is likely indirect perhaps via Cavin-2 (35). In our analysis of isolated DRM from WT and Cav-1 KO mice, only Cavin-1 and Cavin-2 were found to be significantly reduced in Cav-1 KO mice via iTRAQ analysis and semi-quantitative Western blotting thus providing a salient example of the interaction of endogenous Cav-1 with these accessory proteins in vivo. In order to better understand the interactions of caveolins with Cavin-1, velocity sedimentation analysis and cross linking studies were performed. As expected for Cav-1 and Cav-2, they existed as higher order oligomers (>150 kDa), but unexpectedly, Cavin-1 sedimented as a high Mw oligomer, in the absence or presence of endogenous Cav-1. The appearance of higher ordered oligomers of Cavin-1 were independently confirmed in unbroken cells using a cell permeable cross linking approach. Thus, although Cavin-1 can complex and colocalize with Cavin-2 and caveolins, and the loss of either Cavin-1 or caveolins destabilizes the other protein, biochemically, the Cav-1/Cav-2 oligomeric complex is distinct from Cavin-1.

Cavin-1, originally called polymerase I and transcript release factor (PTRF), is a protein that governs the termination of transcription by RNA polymerase I (53), and has been localized to the cytoplasmic face of caveolae (42, 54-55). Cavin-1 is required for the formation of caveolae in cultured cells (12, 14), zebrafish embryos (12) and in all mammalian tissues that have

caveolae (13) and in rodents, the distribution of Cavin-1 coincides with that of caveolins in various tissues (13, 56). Interestingly, Cavin-1 KO exhibit hyperinsulinemia, reduced adiposity, elevated triglycerides and glucose intolerance, phenotypes reminiscent of Cav-1 and/or Cav-3 KO mice. From a mechanistic perspective, it is not known how Cavin-1 functions to regulate the assembly and/or kinectics of caveolae, but recent data suggests that Cavin-2 recruits Cavin-1 to Cav-1/caveolae permitting plasma membrane tubulation events to occur (35).

In the present study, we show that Cavin-1 is highly expressed in EC lining intact blood vessels and in cultured EC, colocalizes with Cav-1 both by sucrose gradient centrifugation and immunoflorescence microscopy and its expression is dependent on the presence of Cav-1 in vitro and in vivo. Reconstitution of Cav-1 using EC specific transgenesis in a Cav-1 KO background partially restores Cavin-1 level in tissues where EC are abundant (lung/aorta) as well as in cultured EC from these animals. Whether the increase in both Cav-1 and Cavin-1 results in increased caveolae structures in EC is not known since we did not quantify the organelle in this study. However, we have previously shown that increasing the levels of Cav-1 over and above endogenous levels does not increase caveolae number in the endothelium by EM (43). A possible explanation of the effects of Cav-1 may be through the stabilization of Cav-2. We have previously shown that Cav-2 and specifically its phosphorylation at serine residues 23 and 36 are positive regulators of caveolae biogenesis (30).

Apart from adipocytes and skeletal muscle, caveolae are highly abundant in EC (3) and there are major cardiovascular phenotypes in Cav-1 KO mice such as defects in vascular function, angiogenesis, cardiac hypertrophy and pulmonary hypertension. Mechanistically, the impaired vascular and pulmonary functions are due to dysregulation of endothelial nitric oxide synthase (eNOS) resulting in enhanced NO levels in Cav-1 KO mice (8, 20-22). Here, we show

a reduction in Cavin-1 increases NO production in EC and this is due presumably to the loss of the inhibitory influence of Cav-1 on eNOS. Also, a reduction in Cavin-1 reduced several in vitro paradigms of angiogenesis including EC proliferation, migration and cord formation. Although the loss of Cav-1 can promote cell growth (21) it can stimulate or inhibit angiogenesis(57-58), thus, it is possible that the decrease in angiogenic phenotypes after knockdown of Cavin-1 may be reflect the complex actions of Cav-1 or be independent of Cav-1 and relate to its action in transcriptional termination processes (53).

In summary, using a comparative quantitative proteomic analysis of proteins within Cav-1 enriched membranes of intact tissue, we have identified and characterized the role of Cavin-1 in EC. Additional analysis are required to elucidate the relationships between Cav-1, Cavins and intracellular targets such as eNOS and to characterize the relevance of proteins enriched in DRM after the loss of Cav-1.

REFERENCES

1. Parton, R. G., and Simons, K. (2007) The multiple faces of caveolae. *Nat Rev Mol Cell Biol* **8**, 185-194.

2. Pilch, P. F., Souto, R. P., Liu, L., Jedrychowski, M. P., Berg, E. A., Costello, C. E., and Gygi, S. P. (2007) Cellular spelunking: exploring adipocyte caveolae. *J Lipid Res* **48**, 2103-2111.

3. Gratton, J. P., Bernatchez, P., and Sessa, W. C. (2004) Caveolae and caveolins in the cardiovascular system. *Circ Res* **94**, 1408-1417.

4. Cohen, A. W., Hnasko, R., Schubert, W., and Lisanti, M. P. (2004) Role of caveolae and caveolins in health and disease. *Physiol Rev* **84**, 1341-1379.

5. Frank, P. G., Pavlides, S., Cheung, M. W., Daumer, K., and Lisanti, M. P. (2008) Role of caveolin-1 in the regulation of lipoprotein metabolism. *Am J Physiol Cell Physiol* **295**, C242-248.

6. Frank, P. G., Pavlides, S., and Lisanti, M. P. (2009) Caveolae and transcytosis in endothelial cells: role in atherosclerosis. *Cell Tissue Res* **335**, 41-47.

7. Fernandez-Hernando, C., Ackah, E., Yu, J., Suarez, Y., Murata, T., Iwakiri, Y., Prendergast, J., Miao, R. Q., Birnbaum, M. J., and Sessa, W. C. (2007) Loss of Akt1 leads to severe atherosclerosis and occlusive coronary artery disease. *Cell Metab* **6**, 446-457.

8. Drab, M., Verkade, P., Elger, M., Kasper, M., Lohn, M., Lauterbach, B., Menne, J., Lindschau, C., Mende, F., Luft, F. C., Schedl, A., Haller, H., and Kurzchalia, T. V. (2001) Loss of caveolae, vascular dysfunction, and pulmonary defects in caveolin-1 gene-disrupted mice. *Science* **293**, 2449-2452.

9. Fra, A. M., Williamson, E., Simons, K., and Parton, R. G. (1995) De novo formation of caveolae in lymphocytes by expression of VIP21-caveolin. *Proc Natl Acad Sci USA* **92**, 8655-8659.

10. Galbiati, F., Engelman, J. A., Volonte, D., Zhang, X. L., Minetti, C., Li, M., Hou, H., Jr., Kneitz, B., Edelmann, W., and Lisanti, M. P. (2001) Caveolin-3 null mice show a loss of caveolae, changes in the microdomain distribution of the dystrophin-glycoprotein complex, and t-tubule abnormalities. *J Biol Chem* **276**, 21425-21433.

11. Razani, B., Wang, X. B., Engelman, J. A., Battista, M., Lagaud, G., Zhang, X. L., Kneitz, B., Hou, H., Jr., Christ, G. J., Edelmann, W., and Lisanti, M. P. (2002) Caveolin-2-deficient mice show evidence of severe pulmonary dysfunction without disruption of caveolae. *Mol Cell Biol* **22**, 2329-2344.

12. Hill, M. M., Bastiani, M., Luetterforst, R., Kirkham, M., Kirkham, A., Nixon, S. J., Walser, P., Abankwa, D., Oorschot, V. M., Martin, S., Hancock, J. F., and Parton, R. G. (2008) PTRF-Cavin, a conserved cytoplasmic protein required for caveola formation and function. *Cell* **132**, 113-124.

13. Liu, L., Brown, D., McKee, M., Lebrasseur, N. K., Yang, D., Albrecht, K. H., Ravid, K., and Pilch, P. F. (2008) Deletion of Cavin/PTRF causes global loss of caveolae, dyslipidemia, and glucose intolerance. *Cell Metab* **8**, 310-317.

14. Liu, L., and Pilch, P. F. (2008) A critical role of cavin (polymerase I and transcript release factor) in caveolae formation and organization. *J Biol Chem* **283**, 4314-4322.

15. Ross, P. L., Huang, Y. N., Marchese, J. N., Williamson, B., Parker, K., Hattan, S., Khainovski, N., Pillai, S., Dey, S., Daniels, S., Purkayastha, S., Juhasz, P., Martin, S., Bartlet-Jones, M., He, F., Jacobson, A., and Pappin, D. J. (2004) Multiplexed protein quantitation in

Saccharomyces cerevisiae using amine-reactive isobaric tagging reagents. *Mol Cell Proteomics* **3**, 1154-1169.

16. Guo, Y., Singleton, P. A., Rowshan, A., Gucek, M., Cole, R. N., Graham, D. R., Van Eyk, J. E., and Garcia, J. G. (2007) Quantitative proteomics analysis of human endothelial cell membrane rafts: evidence of MARCKS and MRP regulation in the sphingosine 1-phosphate-induced barrier enhancement. *Mol Cell Proteomics* **6**, 689-696.

17. Ralhan, R., Desouza, L. V., Matta, A., Chandra Tripathi, S., Ghanny, S., Datta Gupta, S., Bahadur, S., and Siu, K. W. (2008) Discovery and verification of head-and-neck cancer biomarkers by differential protein expression analysis using iTRAQ labeling, multidimensional liquid chromatography, and tandem mass spectrometry. *Mol Cell Proteomics* **7**, 1162-1173.

18. Frank, P. G., Woodman, S. E., Park, D. S., and Lisanti, M. P. (2003) Caveolin, caveolae, and endothelial cell function. *Arterioscler Thromb Vasc Biol* **23**, 1161-1168.

19. Stan, R. V., Roberts, W. G., Predescu, D., Ihida, K., Saucan, L., Ghitescu, L., and Palade, G. E. (1997) Immunoisolation and partial characterization of endothelial plasmalemmal vesicles (caveolae). *Mol Biol Cell* **8**, 595-605.

20. Murata, T., Lin, M. I., Huang, Y., Yu, J., Bauer, P. M., Giordano, F. J., and Sessa, W. C. (2007) Reexpression of caveolin-1 in endothelium rescues the vascular, cardiac, and pulmonary defects in global caveolin-1 knockout mice. *J Exp Med* **204**, 2373-2382.

21. Razani, B., Engelman, J. A., Wang, X. B., Schubert, W., Zhang, X. L., Marks, C. B., Macaluso, F., Russell, R. G., Li, M., Pestell, R. G., Di Vizio, D., Hou, H., Jr., Kneitz, B., Lagaud, G., Christ, G. J., Edelmann, W., and Lisanti, M. P. (2001) Caveolin-1 null mice are viable but show evidence of hyperproliferative and vascular abnormalities. *J Biol Chem* **276**, 38121-38138.

22. Yu, J., Bergaya, S., Murata, T., Alp, I. F., Bauer, M. P., Lin, M. I., Drab, M., Kurzchalia, T. V., Stan, R. V., and Sessa, W. C. (2006) Direct evidence for the role of caveolin-1 and caveolae in mechanotransduction and remodeling of blood vessels. *J Clin Invest* **116**, 1284-1291.

23. Abrami, L., Fivaz, M., Kobayashi, T., Kinoshita, T., Parton, R. G., and van der Goot, F. G. (2001) Cross-talk between caveolae and glycosylphosphatidylinositol-rich domains. *J Biol Chem* **276**, 30729-30736.

24. Keller, A., Nesvizhskii, A. I., Kolker, E., and Aebersold, R. (2002) Empirical statistical model to estimate the accuracy of peptide identifications made by MS/MS and database search. *Anal Chem* **74**, 5383-5392.

25. Nesvizhskii, A. I., Keller, A., Kolker, E., and Aebersold, R. (2003) A statistical model for identifying proteins by tandem mass spectrometry. *Anal Chem* **75**, 4646-4658.

26. Shilov, I. V., Seymour, S. L., Patel, A. A., Loboda, A., Tang, W. H., Keating, S. P., Hunter, C. L., Nuwaysir, L. M., and Schaeffer, D. A. (2007) The Paragon Algorithm, a next generation search engine that uses sequence temperature values and feature probabilities to identify peptides from tandem mass spectra. *Mol Cell Proteomics* **6**, 1638-1655.

27. Salim, K., Kehoe, L., Minkoff, M. S., Bilsland, J. G., Munoz-Sanjuan, I., and Guest, P. C. (2006) Identification of differentiating neural progenitor cell markers using shotgun isobaric tagging mass spectrometry. *Stem Cells Dev* **15**, 461-470.

28. Seshi, B. (2006) An integrated approach to mapping the proteome of the human bone marrow stromal cell. *Proteomics* **6**, 5169-5182.

29. Sargiacomo, M., Scherer, P. E., Tang, Z., Kubler, E., Song, K. S., Sanders, M. C., and Lisanti, M. P. (1995) Oligomeric structure of caveolin: implications for caveolae membrane organization. *Proc Natl Acad Sci USA* **92**, 9407-9411.

30. Sowa, G., Pypaert, M., Fulton, D., and Sessa, W. C. (2003) The phosphorylation of caveolin-2 on serines 23 and 36 modulates caveolin-1-dependent caveolae formation. *Proc Natl Acad Sci USA* **100**, 6511-6516.

31. Litman, T., Jensen, U., Hansen, A., Covitz, K. M., Zhan, Z., Fetsch, P., Abati, A., Hansen, P. R., Horn, T., Skovsgaard, T., and Bates, S. E. (2002) Use of peptide antibodies to probe for the mitoxantrone resistance-associated protein MXR/BCRP/ABCP/ABCG2. *Biochim Biophys Acta* **1565**, 6-16.

32. Fulton, D., Gratton, J. P., McCabe, T. J., Fontana, J., Fujio, Y., Walsh, K., Franke, T. F., Papapetropoulos, A., and Sessa, W. C. (1999) Regulation of endothelium-derived nitric oxide production by the protein kinase Akt. *Nature* **399**, 597-601.

33. Foster, L. J., De Hoog, C. L., and Mann, M. (2003) Unbiased quantitative proteomics of lipid rafts reveals high specificity for signaling factors. *Proc Natl Acad Sci USA* **100**, 5813-5818.

34. Zheng, Y. Z., Berg, K. B., and Foster, L. J. (2009) Mitochondria do not contain lipid rafts, and lipid rafts do not contain mitochondrial proteins. *J Lipid Res* **50**, 988-998.

35. Hansen, C. G., Bright, N. A., Howard, G., and Nichols, B. J. (2009) SDPR induces membrane curvature and functions in the formation of caveolae. *Nat Cell Biol* **11**, 807-814.

36. Mineo, C., Ying, Y. S., Chapline, C., Jaken, S., and Anderson, R. G. (1998) Targeting of protein kinase Calpha to caveolae. *J Cell Biol* **141**, 601-610.

37. Rahman, A., and Sward, K. (2009) The role of caveolin-1 in cardiovascular regulation. *Acta Physiol (Oxf)* **195**, 231-245.

38. Fernandez-Hernando, C., Yu, J., Suarez, Y., Rahner, C., Davalos, A., Lasuncion, M. A., and Sessa, W. C. (2009) Genetic evidence supporting a critical role of endothelial caveolin-1 during the progression of atherosclerosis. *Cell Metab* **10**, 48-54.

39. Song, K. S., Scherer, P. E., Tang, Z., Okamoto, T., Li, S., Chafel, M., Chu, C., Kohtz, D. S., and Lisanti, M. P. (1996) Expression of caveolin-3 in skeletal, cardiac, and smooth muscle cells. Caveolin-3 is a component of the sarcolemma and co-fractionates with dystrophin and dystrophin-associated glycoproteins. *J Biol Chem* **271**, 15160-15165.

40. Pelkmans, L., Burli, T., Zerial, M., and Helenius, A. (2004) Caveolin-stabilized membrane domains as multifunctional transport and sorting devices in endocytic membrane traffic. *Cell* **118**, 767-780.

41. Tagawa, A., Mezzacasa, A., Hayer, A., Longatti, A., Pelkmans, L., and Helenius, A. (2005) Assembly and trafficking of caveolar domains in the cell: caveolae as stable, cargo-triggered, vesicular transporters. *J Cell Biol* **170**, 769-779.

42. Aboulaich, N., Vainonen, J. P., Stralfors, P., and Vener, A. V. (2004) Vectorial proteomics reveal targeting, phosphorylation and specific fragmentation of polymerase I and transcript release factor (PTRF) at the surface of caveolae in human adipocytes. *Biochem J* **383**, 237-248.

43. Bauer, P. M., Yu, J., Chen, Y., Hickey, R., Bernatchez, P. N., Looft-Wilson, R., Huang, Y., Giordano, F., Stan, R. V., and Sessa, W. C. (2005) Endothelial-specific expression of caveolin-1 impairs microvascular permeability and angiogenesis. *Proc Natl Acad Sci USA* **102**, 204-209.

44. Das, K., Lewis, R. Y., Scherer, P. E., and Lisanti, M. P. (1999) The membrane-spanning domains of caveolins-1 and -2 mediate the formation of caveolin hetero-oligomers. Implications for the assembly of caveolae membranes in vivo. *J Biol Chem* **274**, 18721-18728.

45. Li, S., Galbiati, F., Volonte, D., Sargiacomo, M., Engelman, J. A., Das, K., Scherer, P. E., and Lisanti, M. P. (1998) Mutational analysis of caveolin-induced vesicle formation. Expression of caveolin-1 recruits caveolin-2 to caveolae membranes. *FEBS Lett* **434**, 127-134.

46. Hayer, A., Stoeber, M., Bissig, C., and Helenius, A. (2010) Biogenesis of caveolae: stepwise assembly of large caveolin and cavin complexes. *Traffic* **11**, 361-382.

47. Garcia-Cardena, G., Martasek, P., Masters, B. S., Skidd, P. M., Couet, J., Li, S., Lisanti, M. P., and Sessa, W. C. (1997) Dissecting the interaction between nitric oxide synthase (NOS) and caveolin. Functional significance of the nos caveolin binding domain in vivo. *J Biol Chem* **272**, 25437-25440.

48. Michel, J. B., Feron, O., Sacks, D., and Michel, T. (1997) Reciprocal regulation of endothelial nitric-oxide synthase by Ca2+-calmodulin and caveolin. *J Biol Chem* **272**, 15583-15586.

49. Baruthio, F., Quadroni, M., Ruegg, C., and Mariotti, A. (2008) Proteomic analysis of membrane rafts of melanoma cells identifies protein patterns characteristic of the tumor progression stage. *Proteomics* **8**, 4733-4747.

50. von Haller, P. D., Donohoe, S., Goodlett, D. R., Aebersold, R., and Watts, J. D. (2001) Mass spectrometric characterization of proteins extracted from Jurkat T cell detergent-resistant membrane domains. *Proteomics* **1**, 1010-1021.

51. Zheng, Y. Z., and Foster, L. J. (2009) Contributions of quantitative proteomics to understanding membrane microdomains. *J Lipid Res **50**, 1976-1985*.

52. Bastiani, M., Liu, L., Hill, M. M., Jedrychowski, M. P., Nixon, S. J., Lo, H. P., Abankwa, D., Luetterforst, R., Fernandez-Rojo, M., Breen, M. R., Gygi, S. P., Vinten, J., Walser, P. J.,

North, K. N., Hancock, J. F., Pilch, P. F., and Parton, R. G. (2009) MURC/Cavin-4 and cavin family members form tissue-specific caveolar complexes. *J Cell Biol* **185**, 1259-1273.

53. Jansa, P., Mason, S. W., Hoffmann-Rohrer, U., and Grummt, I. (1998) Cloning and functional characterization of PTRF, a novel protein which induces dissociation of paused ternary transcription complexes. *EMBO J* **17**, 2855-2864.

54. Vinten, J., Johnsen, A. H., Roepstorff, P., Harpoth, J., and Tranum-Jensen, J. (2005) Identification of a major protein on the cytosolic face of caveolae. *Biochim Biophys Acta* **1717**, 34-40.

55. Vinten, J., Voldstedlund, M., Clausen, H., Christiansen, K., Carlsen, J., and Tranum-Jensen, J. (2001) A 60-kDa protein abundant in adipocyte caveolae. *Cell Tissue Res* **305**, 99-106.

56. Voldstedlund, M., Vinten, J., and Tranum-Jensen, J. (2001) cav-p60 expression in rat muscle tissues. Distribution of caveolar proteins. *Cell Tissue Res* **306**, 265-276.

57. Williams, T. M., Medina, F., Badano, I., Hazan, R. B., Hutchinson, J., Muller, W. J., Chopra, N. G., Scherer, P. E., Pestell, R. G., and Lisanti, M. P. (2004) Caveolin-1 gene disruption promotes mammary tumorigenesis and dramatically enhances lung metastasis in vivo. Role of Cav-1 in cell invasiveness and matrix metalloproteinase (MMP-2/9) secretion. *J Biol Chem* **279**, 51630-51646.

58. Lin, M. I., Yu, J., Murata, T., and Sessa, W. C. (2007) Caveolin-1-deficient mice have increased tumor microvascular permeability, angiogenesis, and growth. *Cancer Res* **67**, 2849-2856.

AKNOWLEDGEMENTS

We would like to thank Dr. Kenneth Williams for his insights and support for this project. This work was supported by grants R01 HL64793, R01 HL61371, R01 HL081190, P01 Hl70295 and Contract No. N01-HV-28186 (NHLBI-Yale Proteomics Contract) from the National Institutes of Health to W.C. Sessa, and by a Scientist Development Grant from American Heart Association to C. Fernández-Hernando. A Dávalos is a recipient of a postdoctoral fellowship from the Instituto de Salud Carlos III, Spain.

FIGURE LEGENDS

Figure 1. iTRAQ based approach to quantitative analysis of lung proteins within caveolar membrane rafts. Mice lung membrane raft fractions from caveolin-1 KO and WT animals were isolated by solubilization by Triton X-100 at 4°C and after centrifugation, 12 sucrose-gradient fractions were collected and analyzed by immunobloting. Raft fractions 1 and 2 were labeled with iTRAQ reagents and analysis by LC/MS/MS. (B) Number of proteins identified in lung DRMs of WT and Cav-1 KO mice. Three set of experiments by duplicate were performed and common proteins were analyzed for quantitative differences. (C) $Log_{(2)}$ transformed values of the normalized data from ratio WT/KO and internal replicate for the means of the relative protein expression levels. (D) Western blot confirmation of proteins levels reduced in raft fractions of Cav-1 KO mice lung (fractions 1 and 2). Flotillin-1 was used as raft protein marker. (E) Lung tissue lisate from cav-1 KO animals from different age were separated by SDS-PAGE and analyzed by immunobloting for caveolins and cavin levels.

Figure 2. Cavin-1 levels are regulated by Cav-1 in the endothelium. (A) Cavin-1 is found in intact blood vessels. Representative immunofluorescence analysis of serial cross-sections (10 μm) from the mouse aorta stained for Cavin-1 (green), DAPI (for nuclei, blue) and Cav-1(red) in vessels from WT and Cav-1KO mice. The scale bar represent100 μm. (B)Levels of eNOS, Hsp90 (loading control), caveolins-1 and-2 and Cavin-1 proteins in heart, lung and aortic extracts from WT, Cav-1 KO and Cav-1 RC mice. (C) Protein levels of Cavin-1 and caveolins in EC isolated from WT, Cav-1 KO and Cav-1 RC mice as quantified in inset. (D) Cavin-1 and caveolin localization to raft membrane fractions analyzed by sucrose gradient fractionation of EC isolated from WT, Cav-1 KO, Cav-1 RC mice. β-cop and HSP90 were used as markers for non-

raft fractions. (E) Cavin-1 and caveolin levels in EC isolated from control (WT) and transgenic mice overexpressing Cav-1 (Cav-1 TG) in the endothelium. Data are the mean ± SEM of three independent experiments. *P<0.05 vs control (WT).

Figure 3. Characterization of Cavin-1 silencing in human EC. Cavin-1 silencins in (A) Eahy926 cells and (B) HUVEC. Cells were transfected with NS or with 2 independent siRNAs for Cavin-1 (siRNA-1 or siRNA-2) and at indicated time points protein levels were evaluated by immunoblotting. (C) Immunoflorescence microscopy of Cavin-1 (green) in Eahy926 cells in the absence or presence of Cavin-1 siRNA treatment. Blue reflects DAPI staining of nuclei and the scale bar represent 25μm. (D) Raft distribution of Cavin-1 and caveolins in control and Cavin-1 silenced Eahy926 cells. β-cop and HSP90 were used as markers for non-raft fractions. (E) Time course of mRNA expression of Cavin-1and caveolins during Cavin-1 silencing. Gene expression data are expressed taking the control as reference (equal to 1). Values are the mean ± SEM of three independent experiments. Comparisons vs. non-silencing (NS): *, P<0.05.

Figure 4. Oligomerization of caveolins and Cavin-1. The oligomerization state of caveolins and Cavin-1 were examined by velocity centrifugation gradients (calibrated with known Mw markers depicted by arrowheads) in extracts from WT (top panel), Cav-1 KO (middle panel) and Cav-1 RC (bottom panel) EC. Right graph denotes the distribution of Cav-1 (white bars) and Cav-2 (black bars) in the gradient. (B) Cavin-1 silencing weakly reduces high molecular weight caveolin oligomers in human EC . (C) In situ oligomerization of Cavin--1 by chemical cross-linking with DSP in intact cells. Arrows indicate Cavin-1 containing oligomers or protein complexes.

Figure 5. Cavin-1 regulates several endothelial cell phenotypes. (A) Cavin-1 silencing (96 h) increases the levels and phosphorylation of eNOS at serine 1177 (p-eNOS) in Eahy926 and HUVEC. Blots are representative of different experiments with similar results. HSP90 is used as a loading control. (B) Loss of Cavin-1 enhances basal nitric oxide release from Eahy926 cells. Total nitrite accumulation was quantified over 8 hrs. Data are the mean ± SEM of 3 independent experiments performed in triplicate. **P*<0.05 vs control (NS). (C) Cavin-1 silencing reduces cell proliferation, (D) migration and (E) tube formation in EC. Data are the mean ± SEM of three independent experiments performed in quadruplicate, comparisons vs control (NS) at each time point. **P*<0.05 vs control (NS).

Figure 1

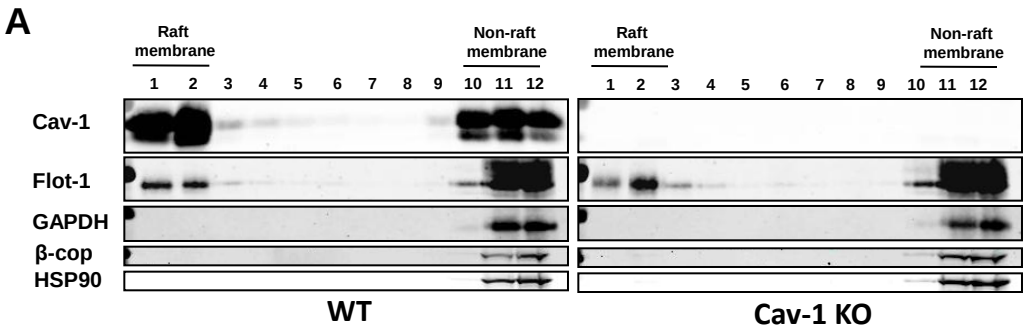
A
Raft membrane
Non-raft membrane
Raft membrane
Non-raft membrane
1 2 3 4 5 6 7 8 9 10 11 12
1 2 3 4 5 6 7 8 9 10 11 12
Cav-1
Flot-1
GAPDH
β-cop
HSP90
WT
Cav-1 KO

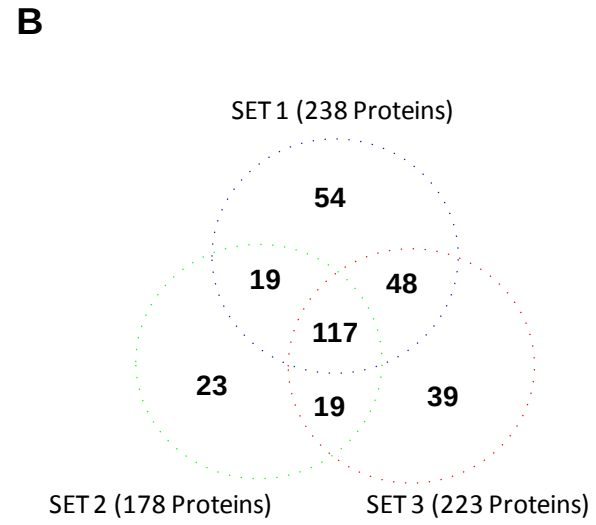
B
SET 1 (238 Proteins)
54
19
48
117
23
19
39
SET 2 (178 Proteins)
SET 3 (223 Proteins)

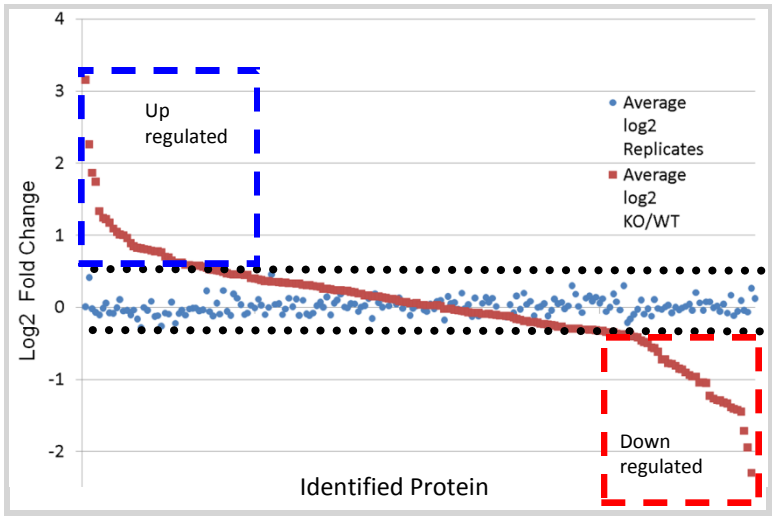
C
Up regulated
Average log2 Replicates
Average log2 KO/WT
Log2 Fold Change
Down regulated
Identified Protein

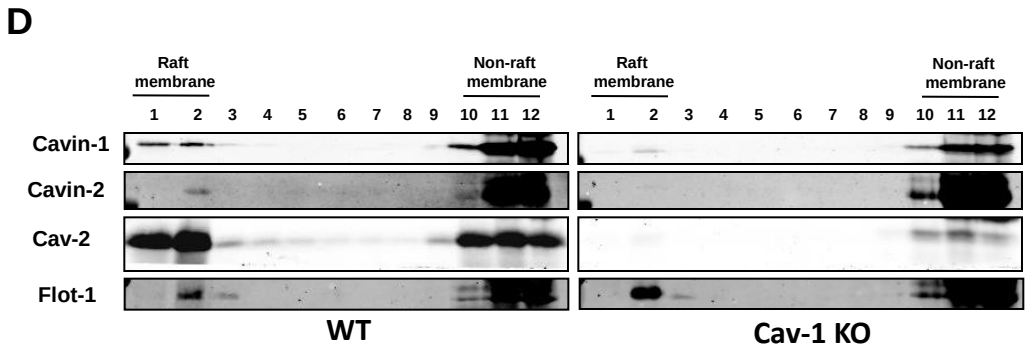
D
Raft membrane
Non-raft membrane
Raft membrane
Non-raft membrane
1 2 3 4 5 6 7 8 9 10 11 12
1 2 3 4 5 6 7 8 9 10 11 12
Cavin-1
Cavin-2
Cav-2
Flot-1
WT
Cav-1 KO

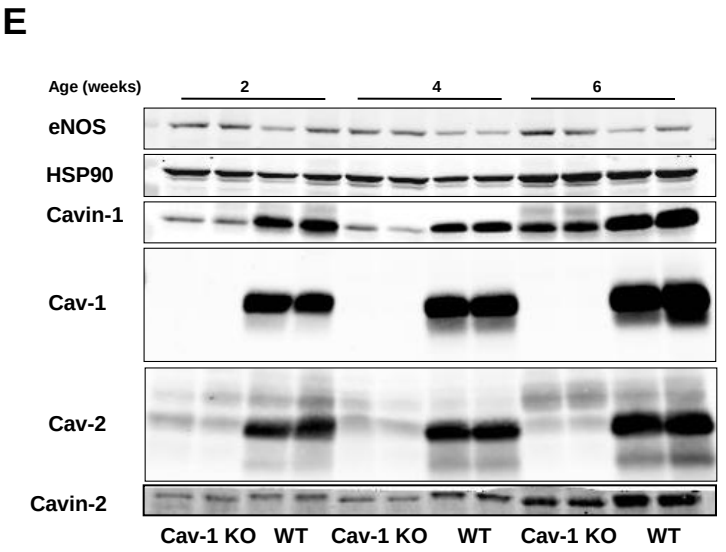
E
Age (weeks)
2
4
6
eNOS
HSP90
Cavin-1
Cav-1
Cav-2
Cavin-2
Cav-1 KO
WT
Cav-1 KO
WT
Cav-1 KO
WT

Figure 2

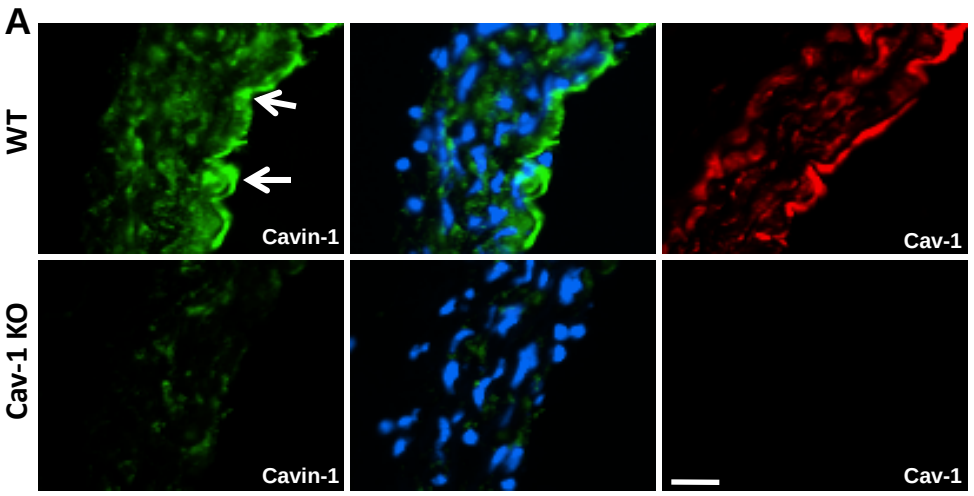
A
WT
Cav-1 KO
Cavin-1
Cav-1
Cavin-1
Cav-1

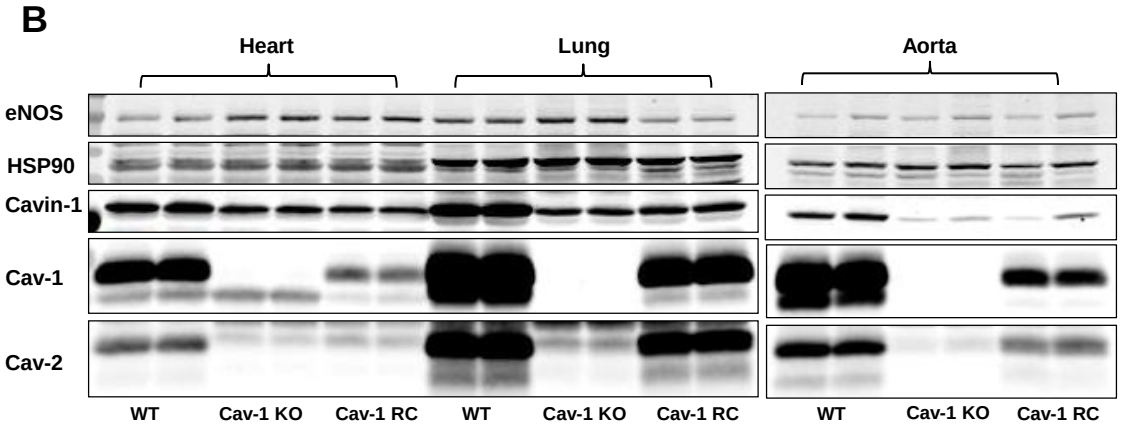
B
Heart
Lung
Aorta
eNOS
HSP90
Cavin-1
Cav-1
Cav-2
WT
Cav-1 KO
Cav-1 RC
WT
Cav-1 KO
Cav-1 RC
WT
Cav-1 KO
Cav-1 RC

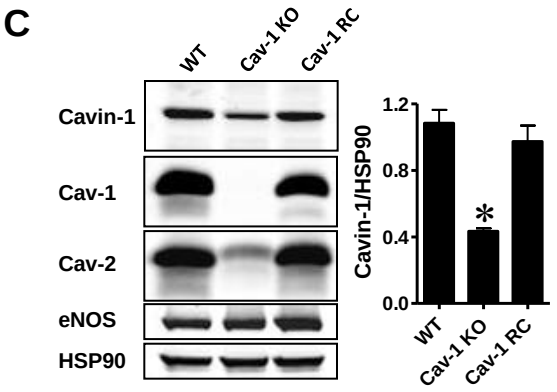
C
WT
Cav-1 KO
Cav-1 RC
Cavin-1
Cav-1
Cav-2
eNOS
HSP90
Cavin-1/HSP90
1.2
0.8
0.4
0.0
*
WT
Cav-1 KO
Cav-1 RC

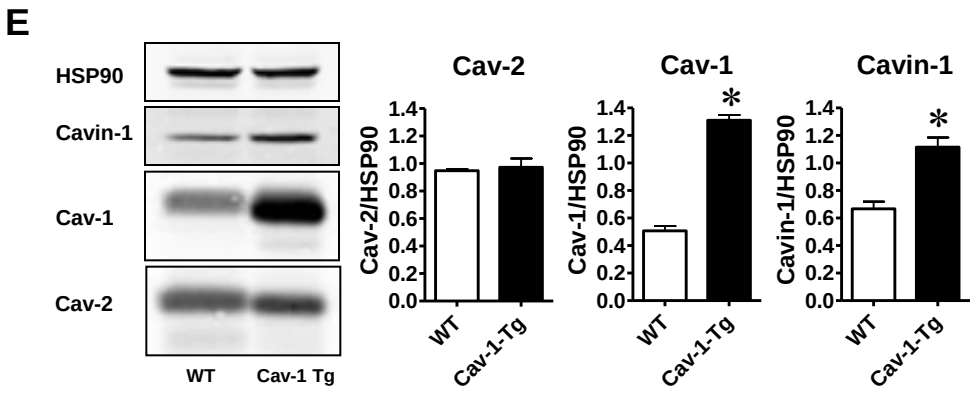
E
HSP90
Cavin-1
Cav-1
Cav-2
WT
Cav-1 Tg
Cav-2
Cav-2/HSP90
Cav-1
Cav-1/HSP90
Cavin-1
Cavin-1/HSP90
1.4
1.2
1.0
0.8
0.6
0.4
0.2
0.0
*
WT
Cav-1-Tg

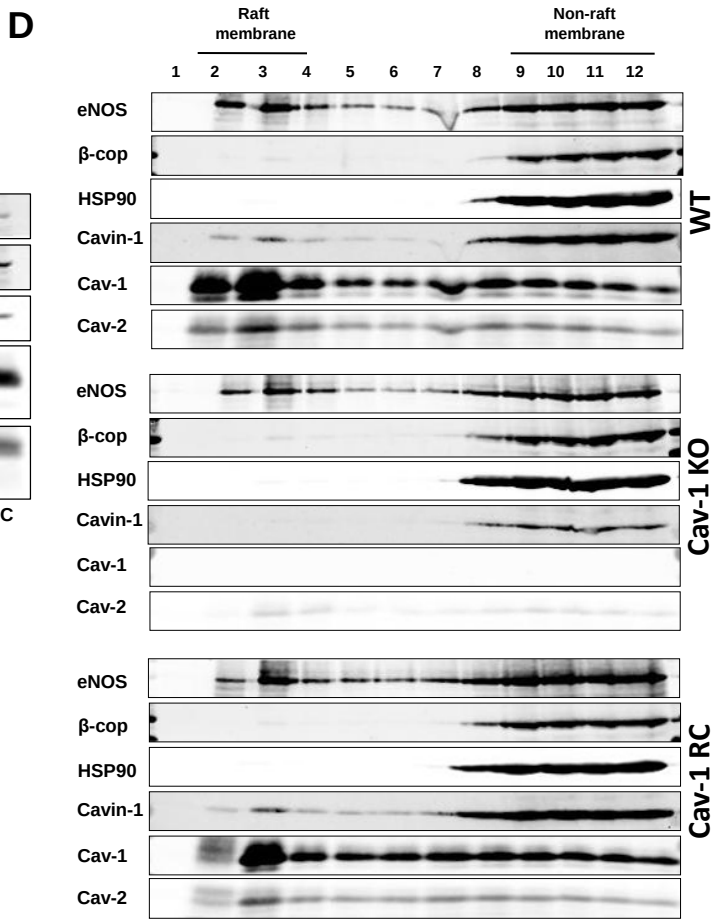
D
Raft membrane
Non-raft membrane
1 2 3 4 5 6 7 8 9 10 11 12
eNOS
β-cop
HSP90
Cavin-1
Cav-1
Cav-2
WT
Cav-1 KO
Cav-1 RC

Figure 3

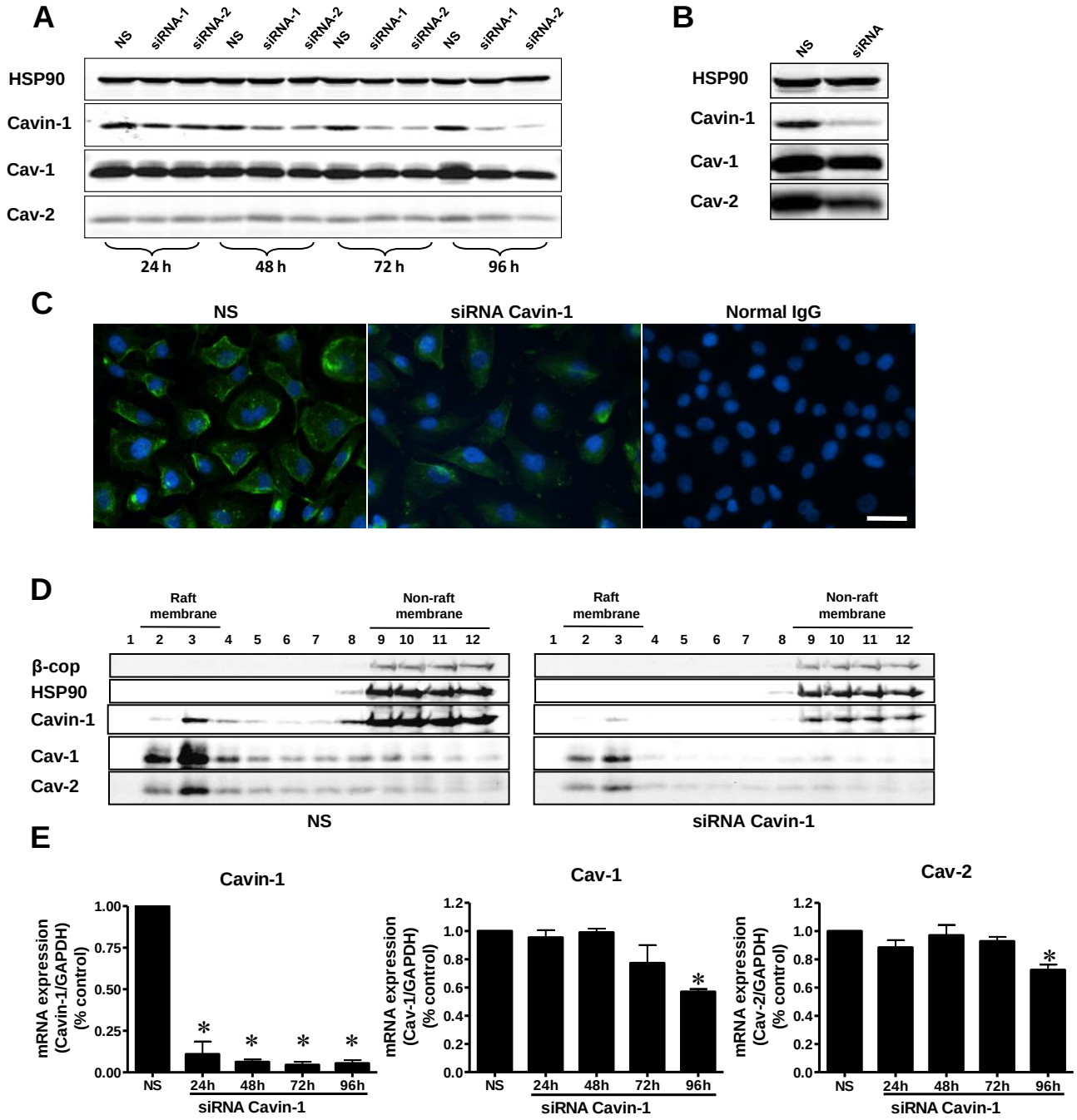
A
NS
siRNA-1
siRNA-2
HSP90
Cavin-1
Cav-1
Cav-2
24 h
48 h
72 h
96 h
B
NS
siRNA
HSP90
Cavin-1
Cav-1
Cav-2
C
NS
siRNA Cavin-1
Normal IgG
D
Raft membrane
Non-raft membrane
1 2 3 4 5 6 7 8 9 10 11 12
β-cop
HSP90
Cavin-1
Cav-1
Cav-2
NS
siRNA Cavin-1
E
Cavin-1
Cav-1
Cav-2
mRNA expression (Cavin-1/GAPDH) (% control)
mRNA expression (Cav-1/GAPDH) (% control)
mRNA expression (Cav-2/GAPDH) (% control)
NS
24h
48h
72h
96h
siRNA Cavin-1

Figure 4

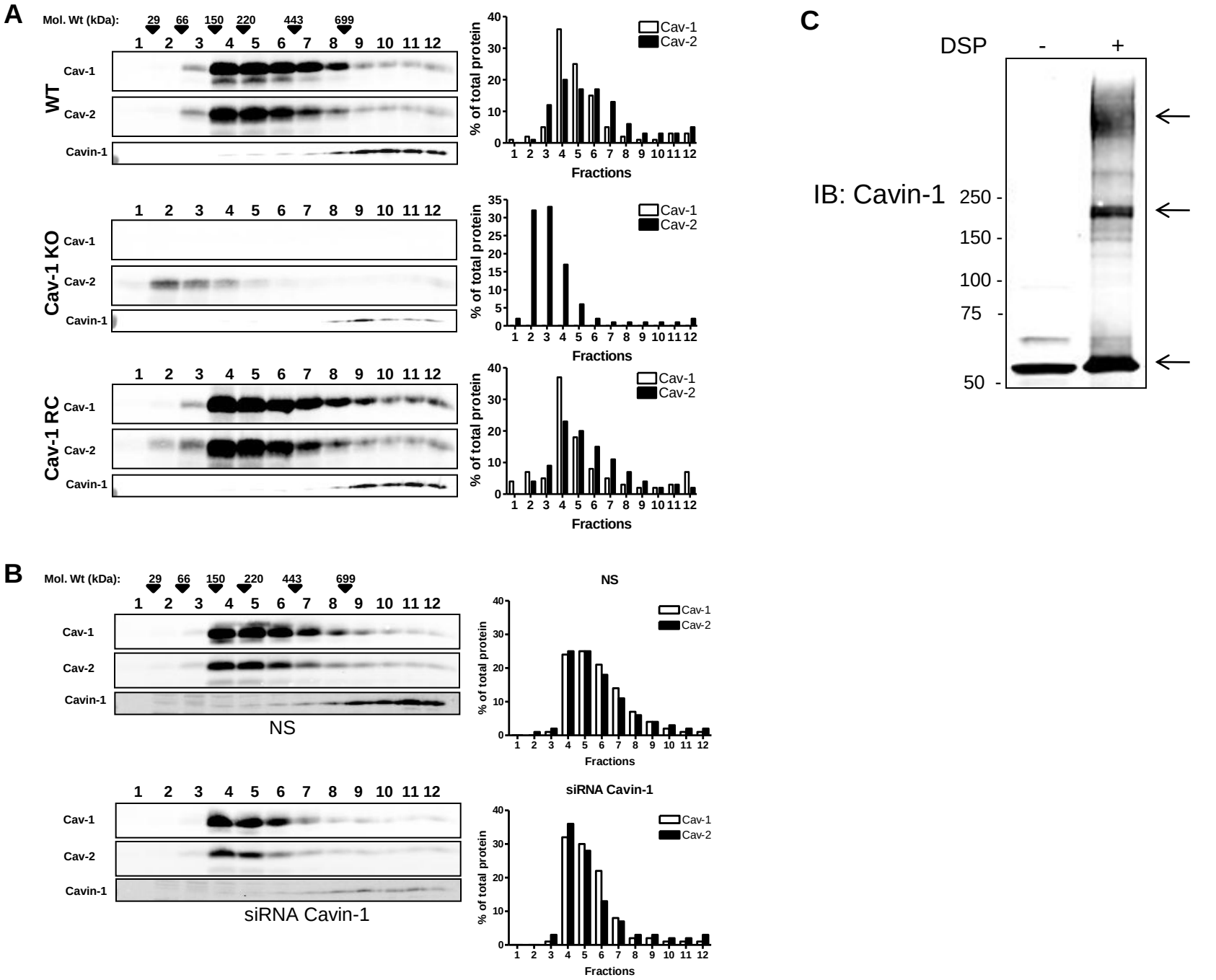
A
Mol. Wt (kDa):
29
66
150
220
443
699
1 2 3 4 5 6 7 8 9 10 11 12
WT
Cav-1 KO
Cav-1 RC
Cav-1
Cav-2
Cavin-1
% of total protein
Fractions
B
NS
siRNA Cavin-1
C
DSP
-
+
IB: Cavin-1
250
150
100
75
50

Figure 5

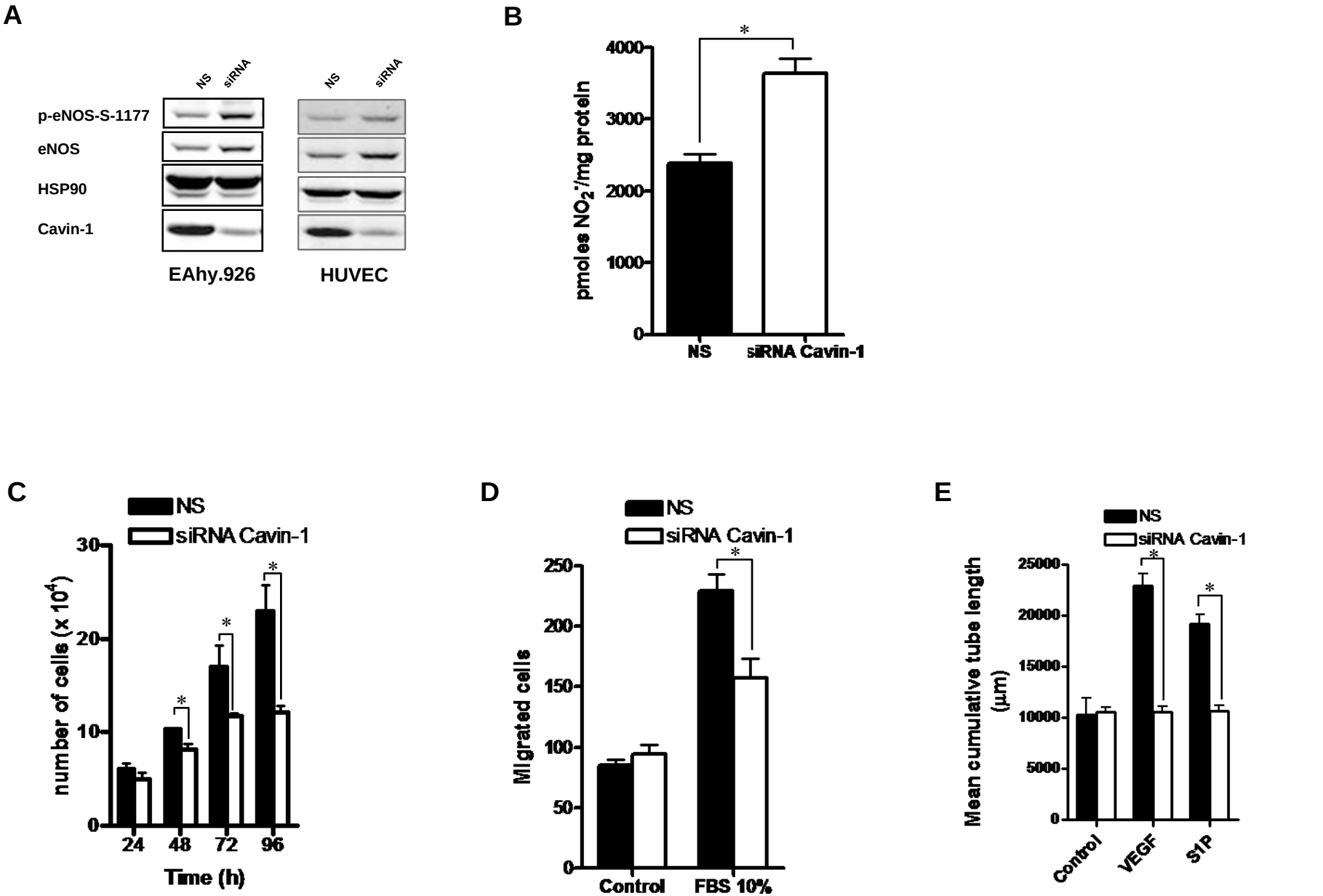
A
NS
siRNA
NS
siRNA
p-eNOS-S-1177
eNOS
HSP90
Cavin-1
EAhy.926
HUVEC
B
*
4000
3000
2000
1000
0
pmoles NO2-/mg protein
NS
siRNA Cavin-1
C
NS
siRNA Cavin-1
30
20
10
0
number of cells (x 10^4)
*
*
*
24
48
72
96
Time (h)
D
NS
siRNA Cavin-1
*
250
200
150
100
50
0
Migrated cells
Control
FBS 10%
E
NS
siRNA Cavin-1
*
*
25000
20000
15000
10000
5000
0
Mean cumulative tube length (µm)
Control
VEGF
S1P

Table 1. Quantitative analysis of proteins reduced in lung membrane rafts of caveolin-1 KO versus WT mice. Fold change reflects data from three independent iTRAQ experiments. Proteins in bold font were confirmed by post-hoc western blotting.

Protein ID	Protein name	# of distinct peptides in ratios	ProteinProphet Score	ProteinPilot Protein Score	Fold change	Grp
IPI00125832	**Caveolin-2**	6	1	2	0.17340	0.005515
IPI00117689	**Polymerase I and transcript release factor (Cavin-1)**	14	1	22.38	0.242523	1.23E-09
IPI00400016	Laminin gamma-1 chain precursor	27	1	56.25	0.332421	1.53E-07
IPI00135660	**Serum deprivation-response protein (SDPR, Cavin-2)**	14	1	23.34	0.356752	1.54E-08
IPI00338452	Collagen alpha-2(IV) chain precursor	27	1	53.35	0.404912	8.81E-09
IPI00119065	Laminin beta-2 chain precursor	22	1	47.94	0.42949	7.08E-09
IPI00117115	Laminin gamma-2 chain precursor	9	1	17.78	0.439639	1.97E-05
IPI00649506	POEM-Nephronectin	11	1	20.88	0.460032	7.16E-07
IPI00229542	Histone protein Hist1h2aa	5	1	11.41	0.487956	9.90E-07
IPI00339885	Collagen alpha-1(VI) chain precursor	7	1	16.15	0.520209	2.22E-05
IPI00222188	Procollagen, type I, alpha 2	50	1	80.49	0.541152	3.40E-06
IPI00223713	Histone H1.2	4	1	7.98	0.57921	6.42E-06
IPI00329872	Isoform 1 of Collagen alpha-1(I) chain precursor	58	1	102.35	0.58872	4.39E-07
IPI00230133	Histone H1.5	3	1	9.13	0.605466	2.29E-05
IPI00753139	AHNAK	2	1	2.13	0.626105	0.003095
IPI00223714	Histone H1.4	4	1	24.08	0.63929	4.29E-05
IPI00553798	AHNAK nucleoprotein isoform 1	263	1	419.45	064112	0.002718
IPI00230702	Icam1	2	0.8	4.34	0.66573	0.047698
IPI00338785	Laminin B1 subunit 1	7	0.94	8.94	0.66879	0.047449
IPI00421223	Tropomyosin alpha-4 chain	7	1	11.81	0.66896	0.007480
IPI00474554	MfAP4	3	1	2.66	0.69693	2.41E-05
IPI00227299	Vimentin	29	1	69.7	0.722867	1.90E-05
IPI00229703	Vesicle-associated membrane protein 2	2	1	7.77	0.733982	0.0001236
IPI00135971	Tight junction protein ZO-1	23	1	38.27	0.740322	0.0319772
IPI00130102	Desmin	9	1	20.79	0.786906	0.0003938

Each protein was identified in three separate biological replicates and by the Paragon and MASCOT database search engines on IPI_mouse database. False discovery rates were determined by running PeptideProphet and ProteinProphet analysis on MASCOT results. Raw data and data results are available at http://yped.med.yale.edu/repository (ACCESS CODE - **aSKezE**)

Table 2. Quantitative analysis of proteins increased in lung membrane rafts of caveolin-1 KO versus WT mice. Fold change reflects data from three independent experiments.

Protein ID	Protein name	# of distinct peptides in ratios	ProteinProphet score	Proteinpilot Protein Score	Fold change	Grp
IPI00323230	Spectrin alpha chain	6	1	218.04	1.214358	1.14E-08
IPI00307966	ADP-ribosyl cyclase 1	11	1	17.07	1.215031	1.63E-07
IPI00117735	Myelin P0 protein precursor	6	1	6.48	1.221400	0.000288
IPI00679092	similar to spectrin alpha 1	5	1	8.36	1.225561	1.75E-08
IPI00131176	Cytochrome c oxidase subunit 2	4	1	8.56	1.243182	0.003629
IPI00109727	Thy-1 membrane glycoprotein precursor	3	1	6	1.261946	0.000248
IPI00123746	Cadherin-13 precursor	10	1	19.23	1.317579	0.000150
IPI00223047	cytoskeleton-associated protein 4	13	1	20.8	1.335605	2.63E-06
IPI00120719	cytochrome c oxidase, subunit Va	20	1	32.69	1.38002	1.03E-05
IPI00131695	Serum albumin precursor	27	1	51.18	1.385615	9.60E-09
IPI00121550	Na/K-transporting ATPase subunit beta-1	5	1	10.26	1.39774	0.001573
IPI00116154	cytochrome c oxidase, subunit Vb	7	1	14	1.42061	1.64E-07
IPI00128642	Lung carbonyl reductase	5	1	12.19	1.446933	9.37E-06
IPI00133956	Gpihbp1	2	1	3.1	1.453672	2.84E-05
IPI00225390	Cytochrome c oxidase subunit VIb isoform 1	8	1	16.44	1.460724	6.27E-07
IPI00170093	Ndufs8	5	1	5.73	1.489794	2.96E-05
IPI00121209	Apolipoprotein A-I precursor	25	1	26.07	1.407229	2.56E-05
IPI00121319	Cysteine-rich protein 2	4	0.94	5.55	1.513123	0.000772
IPI00133562	Chchd3	10	1	16.1	1.533374	3.45E-07
IPI00230540	VDAC1	7	1	15.4	1.544335	2.38E-08
IPI00133006	Acyl carrier protein	6	1	10.28	1.562844	2.72E-05
IPI00121288	Ndufb10	2	0.97	4.47	1.641092	2.13E-05
IPI00126208	hemoglobin, beta adult major chain	3	1	14.03	1.66103	8.25E-09
IPI00315480	surfactant associated protein A	13	1	20.97	1.661763	4.56E-05
IPI00132474	Itgb1	8	1	14.96	1.663839	5.88E-07
IPI00311682	Atp1a1	13	1	22.67	1.727181	1.71E-05
IPI00229008	Ndufs4	6	1	11.07	1.81813	8.10E-09
IPI00115522	fibrinogen, alpha polypeptide	3	0.94	5.53	1.915084	4.08E-06
IPI00119618	Calnexin precursor	10	1	20.67	2.138918	0.000461
IPI00316491	Hemoglobin beta-2 subunit	6	1	29.92	2.096561	3.92E-11
IPI00110658	Hemoglobin, beta adult major chain	3	1	18.65	2.17418	5.65E-09
IPI00230113	Cytochrome b5	6	1	10.33	2.204051	1.93E-11
IPI00469114	Hemoglobin alpha subunit	3	1	2.36	2.230882	8.95E-09
IPI00387318	Tmem30a	3	1	5.15	3.114185	5.10E-08
IPI00623553	ATP synthase D chain, mitochondrial	10	1	16.4	3.389328	7.95E-10
IPI00555000	Uqcrb	8	1	10.79	4.012617	1.58E-09

Each protein was identified independently both by Paragon and MASCOT database search engines on IPI_mouse database. False discovery rates were determined by running PeptideProphet and ProteinProphet analysis on MASCOT results. Raw data and data results are available at http://yped.med.yale.edu/repository (ACCESS CODE - **aSKezE**)